Polymer Testing 160 (2026) 109209

Contents lists available at ScienceDirect

Polymer Testing

journal homepage: www.elsevier.com/locate/polytest

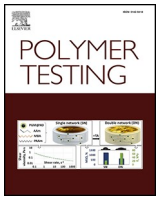

Robust, self-healing polyurea/TPU elastomers

Adriana Nunes dos Santos [a], Mattia Pesce [b], Luca Ceseracciu [c], Martina Nardi [d], Francesca Vasile [e], Ermelinda Falletta [e,f], Alessandro Chiolerio [a,*]

[a] Istituto Italiano di Tecnologia, Bioinspired Soft Robotics, Via Morego 30, Genova, 16163, Italy
[b] Istituto Italiano di Tecnologia, Neuroscience and Brain Technology, Via Morego 30, Genova, 16163, Italy
[c] Istituto Italiano di Tecnologia, Materials Characterization Facility, Via Morego 30, Genova, 16163, Italy
[d] Istituto Italiano di Tecnologia, Smart Materials, Via Morego 30, Genova, 16163, Italy
[e] Department of Chemistry, University of Milan, via C. Golgi 19, Milan, 20133, Italy
[f] Consorzio Interuniversitario Nazionale per la Scienza e Tecnologia dei Materiali (INSTM), via Giusti 9, Florence, 50121, Italy

A B S T R A C T

The development of self-healing materials is essential for advancing sustainable and durable technologies in fields such as soft robotics, wearable devices, and protective coatings. Polyurea (PU) and thermoplastic polyurethane (TPU) elastomers are particularly promising due to their combination of mechanical robustness, flexibility, and industrial processability. In this study, a PU/TPU elastomer was synthesized via the incorporation of polyurea/urethane segments into a commercial TPU matrix, producing a material with a dynamic, hydrogen-bonded network. FTIR analysis confirmed the presence of reversible interactions between urethane and urea groups, which underpin the material's intrinsic self-healing capability. The optimized PU/TPU formulation exhibits exceptional mechanical performance, with a tensile strength of 22.55 MPa, elongation at break of 872%, and toughness of 106.45 MJ m^{-3}. Thermal self-healing tests at 120 °C demonstrated rapid recovery of mechanical properties, achieving healing efficiencies of 34.4%, 76.8%, and 84.2% after 2, 5, and 10 min, respectively. Cyclic tensile tests confirmed the durability and repeatability of self-healing behavior over multiple loading cycles. At the same time, optical microscopy and stress-relaxation experiments provided insight into the kinetics of bond reformation and chain reorganization. These results highlight the potential of PU/TPU elastomers as high-performance, self-healing materials that combine mechanical toughness, extensibility, and rapid repair.

1. Introduction

In recent years, the development of self-healing materials has gained importance in material science, driven by the increasing demand for durable, sustainable, and efficient materials across a wide range of industries [1–4]. Among the most promising candidates for self-healing applications are polyurea (PU) and thermoplastic polyurethane (TPU) elastomers, which combine excellent mechanical properties, flexibility, and industrial versatility [5–7]. However, despite these remarkable qualities, these materials face a critical challenge: their ability to repair the damage while retaining mechanical integrity in an autonomous manner [1,8]. This challenge raises a fundamental question in materials engineering: how can robust mechanical performance be reconciled with effective self-healing functionality?

Although a wide range of self-healing polymers based on dynamic covalent or supramolecular interactions, such as Diels-Alder reactions or hydrogen bonding, have been reported, these materials frequently suffer from reduced mechanical robustness, thermal stability, or chemical resistance when compared to their commercial counterparts [9].

Commercial thermoplastic polyurethanes offer an attractive platform due to their excellent mechanical strength, processability, and industrial scalability. However, their proprietary and fixed molecular architecture hinders direct molecular redesign. To bridge this gap, recent strategies have shifted from backbone modification toward the functionalization of commercial TPUs through the in-situ formation of secondary dynamic architectures. In this context, the incorporation of supramolecular polyurea domains within a TPU matrix enables the introduction of self-healing functionality via reversible interactions while preserving the intrinsic mechanical integrity of the host polymer [10–13].

A key factor influencing the self-healing potential of these materials is the choice of diisocyanate used in their synthesis. Diisocyanates play a crucial role in determining the packing density of the hard segments, which, in turn, affects both the mechanical performance and the self-healing ability of the material. Bulky alicyclic isophorone diisocyanate (IPDI), for instance, has been shown to facilitate looser packing, thereby enhancing the self-healing potential compared to linear aliphatic diisocyanates [14]. This variability in packing density also influences the

* Corresponding author.
E-mail address: alessandro.chiolerio@iit.it (A. Chiolerio).

https://doi.org/10.1016/j.polymertesting.2026.109209
Received 27 October 2025; Received in revised form 30 March 2026; Accepted 4 May 2026
Available online 5 May 2026

formation of hydrogen bonds (HB), one of the most widely studied intrinsic mechanisms for self-healing in elastomers. The ability of hydrogen bonds to form and reform allows for the reorganization of polymer chains, facilitating the self-repair of damage and thereby aiding in the recovery of the material's mechanical properties [15].

In addition to hydrogen bonds, thermal activation has emerged as a critical mechanism for self-healing in elastomers. These materials undergo a physical or chemical transformation that enables the recovery of damaged regions upon thermal activation. This process involves the reversible breaking and reforming of bonds at elevated temperatures, which aids in restoring material integrity. Thermal activation accelerates the healing process by enabling localized heating, which enhances the mobility of polymer chains and promotes the reorganization of hydrogen bonds [16]. This thermal activation mechanism offers a dynamic and efficient method for activating self-healing, allowing the material to recover its mechanical properties [2].

Although research on self-healing elastomers has predominantly focused on polyurethane, polyurea emerges as an alternative due to its simple, fast synthesis and less stringent atmospheric control requirements, as well as the use of widely available precursors such as polyetheramines [14]. For instance, Zhang et al. [8] demonstrated the synthesis of a transparent, elastomeric self-healing polyurea with an elongation of up to 2000%, but with relatively low tensile strength, 1.6 MPa. Strategies such as combining polyurea with commercial TPU have shown potential for increasing tensile strength.

Our aim is the integration of self-healing materials into the fabrication of artificial skins for soft robotics. Materials such as dynamic covalent networks, supramolecular polymers, and ionic elastomers offer autonomous or stimuli-responsive repair mechanisms that enable artificial skins with reversible and repeated repair, emulating the resilience of biological tissues [17]. These materials not only restore mechanical properties like elasticity and flexibility but also critical functionalities such as electrical conductivity, essential for sensory and actuation tasks in soft robotics [18]. Embedding self-healing capabilities at the material level paves the way for more autonomous, durable soft robots capable of reliable operation in dynamic and unpredictable environments [19].

To address these gaps, this study aims to (i) systematically investigate the synthesis and property relationships of PU/TPU blends, (ii) evaluate their self-healing kinetics under thermal activation, including repeated healing cycles, and (iii) quantify the effect of polyurea content on mechanical performance and healing efficiency. These objectives provide a clear roadmap beyond a general investigation of the PU/TPU system, situating this work within the broader context of self-healing elastomer development. The synthesis of this material is characterized by its simplicity, cost-effectiveness, rapidity, and high efficiency, resulting in elastomers with outstanding mechanical properties and significantly enhanced self-healing capabilities.

2. Experimental section

2.1. Materials

IROGRAN A92 P 4637 (polyether-based TPU, Huntsman), isophorone diisocyanate (IPDI, 98%, Sigma-Aldrich), and trimethylolpropane tris[poly(propylene glycol), amine terminated] ether (TTE, Mn 440, Sigma-Aldrich) were used as received. Tetrahydrofuran (THF) was purchased from Sigma-Aldrich and used without further purification.

2.2. Synthesis of polyurea/TPU

The polyurea/TPU self-healing skin was synthesized through the reaction between IROGRAN A92 P4637, isophorone diisocyanate (IPDI), and Trimethylolpropane tris[poly(propylene glycol), amine-terminated] ether (TTE). A stock solution was prepared by dissolving 10 g of TPU in 100 mL of THF. For the synthesis, 2.5 mL of this stock solution (~0.25 g of TPU) was transferred into a 250 mL three-necked flask containing 3 mL of THF under a nitrogen atmosphere. IPDI (0.016 mL) was added, followed by dropwise addition of TTE (0.046 mL). The mixture was stirred at 1400 rpm at room temperature for 2 h. The resulting solution was then poured into a 7 cm diameter Petri dish and left to evaporate at room temperature under a fume hood for 24 h to ensure complete solvent removal. The final material corresponds to a laboratory-scale batch of approximately 0.25 g.

2.3. Characterization and measurements

The presence of the urea group was characterized by Fourier transform infrared spectroscopy (a Vertex 70v FT-IR spectrometer) in a wide wavenumber range of 600-4000 cm^{-1} with a resolution of 4 cm^{-1} using the attenuated total reflection (ATR) mode.

NMR analyses were performed using a Bruker Avance 500 MHz spectrometer equipped with a high-resolution magic angle spinning (HR-MAS) probe, suitable for the characterization of semi-solid and gel-like polymeric systems.

The TPU/PU polymer blend was analyzed in the swollen state using tetrahydrofuran (THF) as solvent. Spectral resolution was enhanced by magic angle spinning (MAS) at a spinning frequency of 5 kHz, allowing effective averaging of anisotropic interactions while preserving solution-like chemical shift information.

All measurements were carried out at a controlled temperature of 303 K.

The following NMR experiments were acquired: ^{1}H NMR, ^{1}H–^{1}H COSY, ^{1}H–^{13}C HSQC, ^{13}C NMR (ZGIG sequence), ^{13}C APT and ^{1}H DOSY (Diffusion-Ordered Spectroscopy).

DOSY experiments were recorded using a pulsed-field gradient stimulated echo sequence with a gradient pulse length p30 = 2.5 ms and a diffusion delay d20 = 100 ms. These parameters were selected to optimize sensitivity to polymer diffusion in the swollen semi-solid state.

The stress–strain curves of the sample were obtained using an Instron 3365 dual-column dynamometer equipped with a 2 KN load cell. Specimens were cut into dogbone shape according to ISO 527 and tested at a rate of 100 mm/min to evaluate the mechanical properties and self-healing ability of the samples. Tensile tests were performed on specimens at different times. The self-healing efficiency (η) was quantified as the ratio of the elongation at break of the healed specimen to that of the original, uncut specimen, expressed as a percentage:

$$\eta = \frac{\text{Elongation at break (healed)}}{\text{Elongation at break (original)}} \times 100\%$$

The healed specimen was prepared by bringing the cut surfaces into contact and subjecting them to a thermal treatment at 120 °C.

The thermal properties of materials were characterized by DMTA (dynamic mechanical thermal analysis) on a TA Instrument Q800 device. Samples were cut into ≈4 mm × 15 mm strips and loaded on the film tension clamp of the instrument. A 15 μm amplitude oscillation was applied at 1 Hz frequency, increasing the temperature from −70 °C to 120 °C with a 3 °C/min heating rate. The output of the tests included the storage modulus, a measure of the conservative part of the material stiffness, and the tanδ, a measure of the relative energy dissipation.

Dogbone samples were stretched cyclically with 20 mm/min rate, 0.2 mm/mm elongation as peak maximum and 0.05 N at peak minimum. This procedure was repeated for 50 cycles. The relative stress relaxation was calculated as a comparative relaxation parameter.

An optical setup (stereomicroscope Nikon SMZ 18, coupled with TP1080HDMI camera) was used to track the healing process of the scratches on the sample surface.

Stress relaxation tests were carried out on a TA Instruments Q800 instrument equipped with a film tension clamp. The samples with dimensions of 25 mm × 4 mm × 0.1 mm were first equilibrated at the initial temperature for 5 min, then a constant deformation of 0.5 % was applied, recording the stress decay as a function of time. The temperature was then increased by 5 °C, and the same procedure was applied.

The tested temperatures were chosen to occur in the rubbery region of the materials (35 °C-55 °C). The normalized stress (G/G_0) was plotted versus time, and the relaxation times (τ) corresponding to 1/e obtained at different temperatures were plotted to calculate the activation energy E_a according to the Arrhenius equation:

$$\ln \tau = \frac{E_a}{RT} - \ln A$$

To complement the mechanical testing, a quantitative image-based analysis was performed using appropriate imaging techniques to monitor the topographical evolution of the damaged interface during the healing process. This analysis was based on time-lapse recordings of the material under thermal activation (120 °C), where image profiles were extracted from cross-sectional views of the damaged region. From these profiles, key morphological features were quantified, namely the peak section area (in μm^2), which reflects the degree of material reconnection, and the full width at half maximum (FWHM), indicative of interface sharpness and heterogeneity. Temperature was measured in real-time using a FLIR E96 camera featuring a 640x480 pixel resolution and extracting information about the region of interest where the sample was located.

3. Results and discussion

3.1. FTIR analysis

As shown in Fig. 1, the neat TPU exhibits a broad absorption peak at 3324 cm^{-1}, corresponding to N–H groups in urethane linkages, and its deformation vibration emerges at 1528 cm^{-1}. Upon blending with polyurea, this band shifted to 3338 cm^{-1} in polyurea/TPU, indicating a partial reorganization of hydrogen bonding interactions due to the incorporation of urea functionalities, which can form intermolecular hydrogen bonds. The absence of the isocyanate band around 2250 cm^{-1} indicates the complete reaction of the isocyanate group [12,20]. Additionally, the characteristic peaks located at 2950 and 2866 cm^{-1} correspond to the asymmetric and symmetric stretching vibrations of the $-CH_2$ groups, respectively [21].

The bands at 1560 cm^{-1} and 1532 cm^{-1} correspond to N–H bending vibrations from hydrogen-bonded and free polyurea groups, respectively [22].

The FTIR results indicate the presence of hydrogen-bonding interactions in the PU/TPU elastomer. To demonstrate the formation of a dynamic hydrogen-bond network, the C=O region of the PU/TPU FTIR spectra (1750–1600 cm^{-1}) was deconvoluted, as shown in Fig. 2. The fitted curve (olive dashed line) follows the experimental spectrum (black continuous line) and confirms that the broad carbonyl band arises from overlapping contributions associated with free and hydrogen-bonded carbonyl groups.

The band at 1729 cm^{-1} is assigned to free urethane C=O groups (cyan component), while the absorption at 1700 cm^{-1} corresponds to disordered hydrogen-bonded carbonyl groups (blue component), and the peak at 1632 cm^{-1} is associated with ordered hydrogen-bonded carbonyls of polyurea (green and red components). These assignments align with previous studies on polyurea systems, which identify three distinct C=O environments: free (non-hydrogen-bonded), disordered (monodentate H-bonding), and ordered (bidentate or highly organized H-bonding) [5,8,23].

The deconvolution reveals that hydrogen-bonded carbonyl species

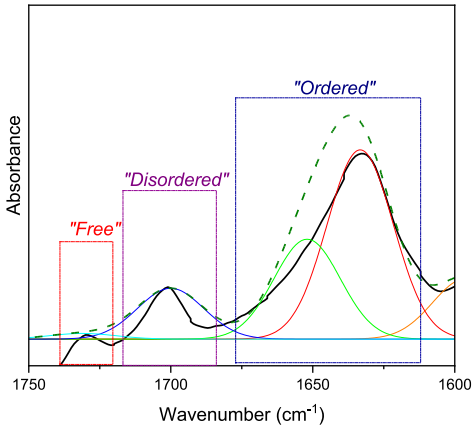

Fig. 2. Results of PU/TPU FTIR spectra in the range of 1750–1600 cm^{-1}.

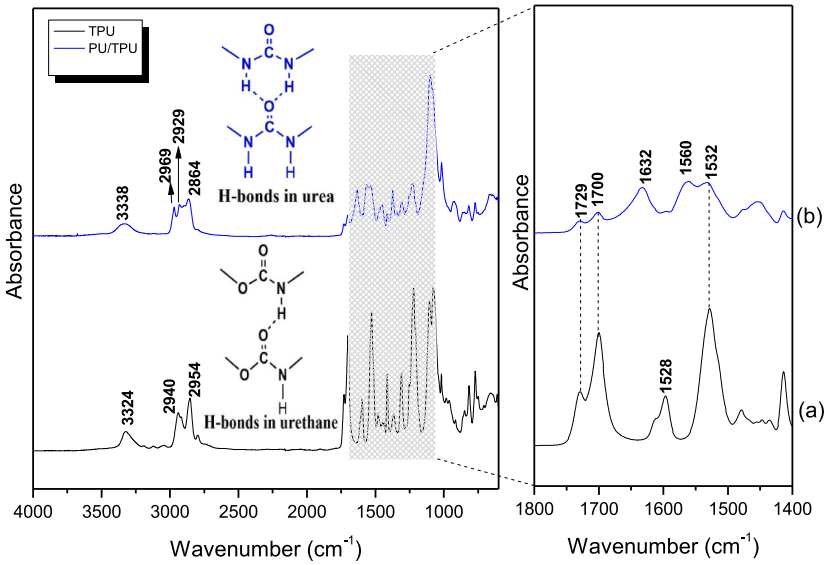

Fig. 1. FTIR spectra of TPU and PU/TPU elastomer.

constitute the major contribution to the carbonyl envelope, while the fraction of free carbonyl groups is comparatively smaller. The coexistence of strongly and weakly hydrogen-bonded carbonyl populations indicates the presence of both stable and dynamic intermolecular interactions within the PU/TPU. Such a distribution supports the existence of a reversible hydrogen-bonding network, which plays a key role in the self-healing behavior of the elastomer.

3.2. NMR analyses

The polymeric material was investigated by high-resolution magic angle spinning (HR-MAS) NMR spectroscopy, which represents a particularly suitable technique for the structural characterization of semi-solid, gel-like, and swollen polymer systems. This approach is especially advantageous for polyurethanes and polyureas, which often display limited solubility and significant line broadening under conventional solid-state or solution NMR conditions. The analyzed material is a commercial polymer, identified by the manufacturer as a polyether-based thermoplastic polyurethane (TPU). As commonly encountered for commercial TPUs, the exact chemical composition and molecular architecture are not fully disclosed, and key parameters such as the molecular weight, molecular weight distribution, and detailed hard/soft segment organization are not available. Consequently, spectroscopic analysis is performed to gain information about the chemical nature of the polymer. Furthermore, several functional groups characteristic of polyurethane and polyurea chemistries exhibit overlapping NMR resonances, both between the two polymer components and with the THF solvent signals used for sample swelling. Consequently, a fully exhaustive structural characterization is not attainable by NMR alone; nevertheless, the acquired spectra provide distinct and meaningful features that allow relevant information to be extracted regarding the chemical nature and predominant polymeric species present in the material.

The ^{1}H HR-MAS NMR spectrum (Fig. 3) of the TPU/PU blend is dominated by resonances characteristic of the polyurethane (TPU) component, indicating that this species is the major constituent of the mixture.

In particular, aromatic proton signals at 7.4 and 7.1 ppm are clearly observed, consistent with aromatic hard segments present in the TPU backbone. Additionally, a distinct urethane NH proton resonance at 8.63 ppm is visible. The integral of this NH signal is coherent with that of the aromatic protons, further supporting the conclusion that the polyurethane represents the predominant polymeric species in the blend.

The ^{13}C HR-MAS NMR spectrum provides further insight into the chemical structure of the polymer blend. In the region corresponding to quaternary carbonyl carbons, a single intense resonance at approximately 153 ppm is observed. This signal is assigned to the urethane carbonyl (–NH–CO–O–) of the polyurethane component.

Importantly, no additional carbonyl resonances attributable to newly formed interfacial functionalities are detected. The absence of multiple carbonyl environments strongly suggests that no grafting reactions occur between the polyurethane and polyurea phases. These observations confirm that the material does not consist of a covalently linked graft copolymer system.

Diffusion-Ordered Spectroscopy (DOSY) was employed to investigate the translational mobility of the polymer species in the swollen state. DOSY NMR separates signals based on their self-diffusion coefficients, providing information on molecular size and dynamic behavior in solution or semi-solid systems.

In polymeric materials, DOSY spectra typically display a distribution of diffusion coefficients, reflecting the inherent polydispersity of polymer chain lengths rather than discrete molecular species. Accordingly, the TPU/PU blend exhibits a diffusion profile characterized by a continuous distribution rather than sharp, single diffusion values.

The DOSY spectrum (Fig. 4) indicates that the polymer signals are predominantly distributed around a diffusion coefficient of approximately 0.8×10^{-10} m^2 s^{-1}.

This value is consistent with the diffusion behavior expected for high-molecular-weight polyurethane chains swollen in THF under HR-MAS conditions.

3.3. Mechanical properties

3.3.1. DMA analysis

The chain mobility and viscoelastic properties of the PU/TPU elastomer were evaluated by measuring the temperature dependence of the storage modulus (E′) and the damping factor (tan δ) via dynamic mechanical analysis (DMA) (Fig. 5). In neat TPU, a single tan δ peak appears at approximately −16 °C, corresponding to the glass transition of

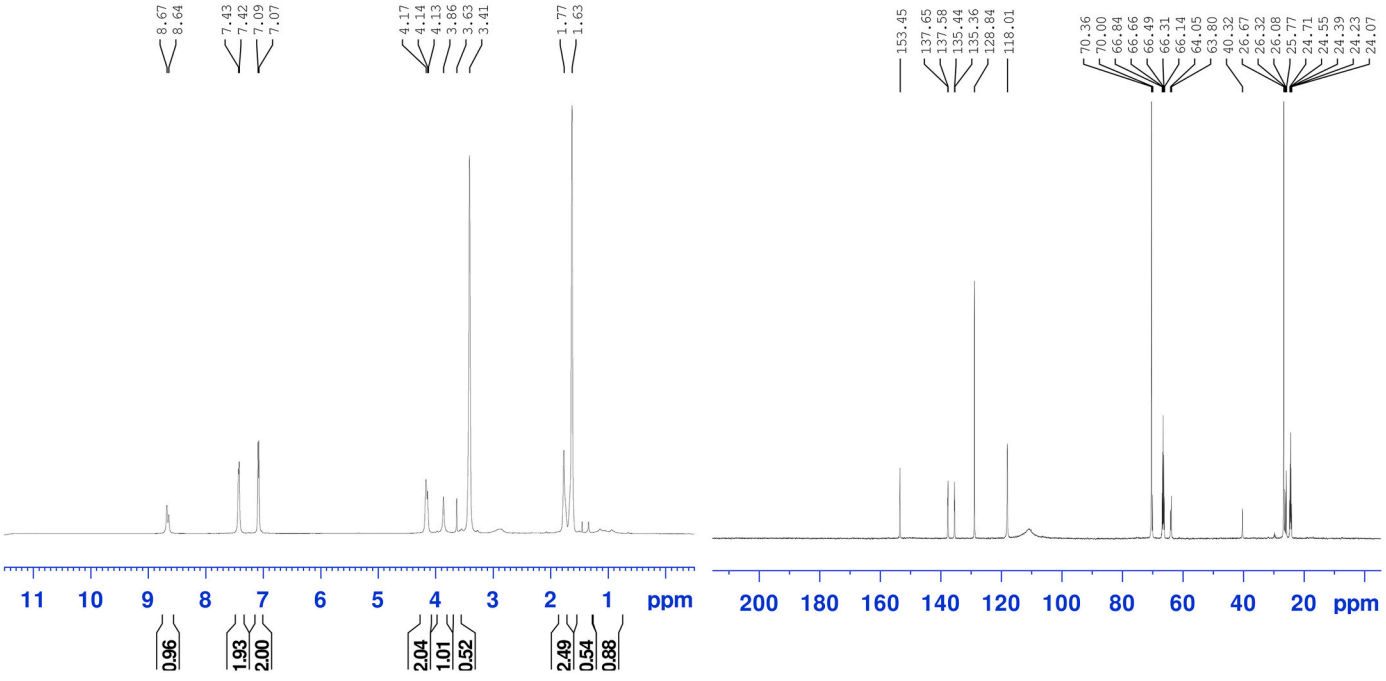

Fig. 3. ^{1}H (left) and ^{13}C (right) HR-MAS NMR spectrum of PU/TPU.

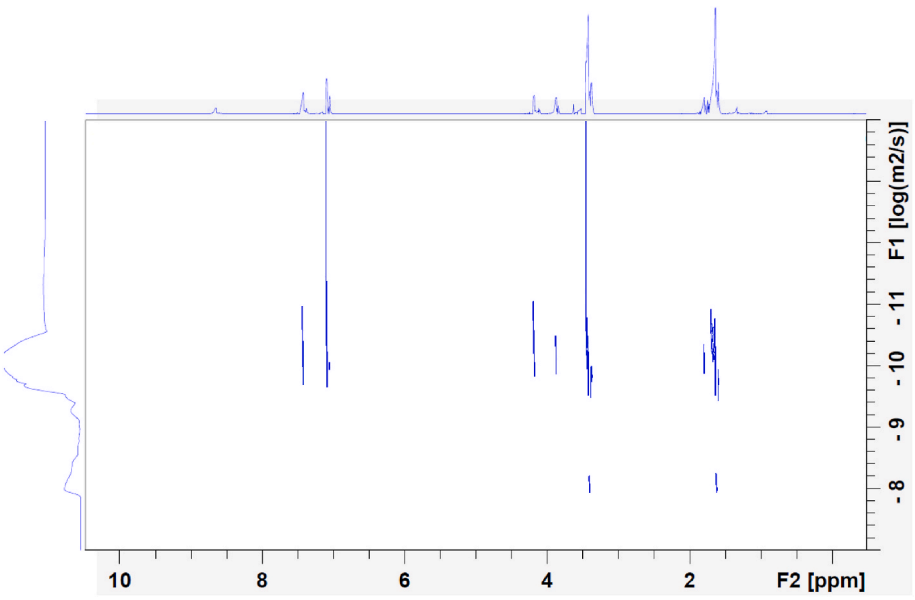

Fig. 4. DOSY spectrum of PU/TPU.

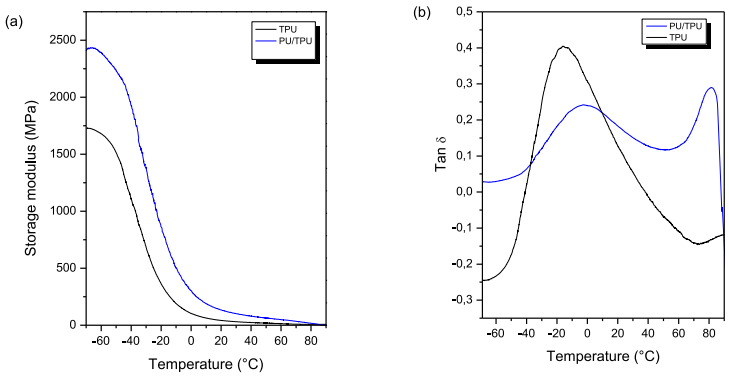

Fig. 5. Temperature dependence of the storage modulus (a) and tan δ (b) of TPU and PU/TPU.

the soft segment. In contrast, the PU/TPU elastomer displays two distinct tan δ peaks at −1.9 °C and 81 °C (Fig. 5b). The lower-temperature peak (−1.9 °C) corresponds to the T_g of the soft TPU-derived phase, shifted to a higher temperature relative to neat TPU, indicative of restricted segmental mobility due to interchain interactions and the formation of reversible hydrogen bonds. The higher-temperature peak (~81 °C) is attributed to the hard domains enriched in polyurea and urethane linkages, which function as transient supramolecular junctions that reinforce the elastomeric network. This dual-transition behavior reflects the microphase-separated architecture of the material, where soft TPU-rich and hard polyurea/urethane-rich domains coexist. Similar observations have been reported in other segmented elastomer systems, such as ethylene-vinyl acetate copolymer/polyurea nanocomposites, where shoulder tan δ peaks arise from strongly intertwined soft and hard phase regions, demonstrating restricted mobility at the interfaces [24].

In storage modulus (E′, Fig. 5a), the PU/TPU system exhibits a higher initial E′ compared to neat TPU, indicating reduced segmental mobility and stronger interchain interactions at low temperatures. Literature on self-healing polyurea elastomers similarly reports increases in E′ and Tg because of dense hydrogen-bonding interactions [25]. In the PU/TPU elastomer, hydrogen bonds (N–H···O=C, N–H···N) formed between urethane and urea groups contribute to a supramolecular network that both stiffens the matrix and introduces dynamic, reversible crosslinks. These interactions suppress soft segment mobility relative to neat TPU, thus shifting the soft Tg and elevating the overall stiffness in both glassy and rubbery regions [8,23].

The gradual decline in E′ with increasing temperature reflects the progressive dissociation of hydrogen bonds and relaxation of the network. However, E′ does not exhibit a sharp drop beyond T_g, suggesting that hard microdomains and residual physical crosslinks persist at elevated temperatures. This behavior is consistent with the presence of ordered hard segments that serve as mechanical reinforcements while maintaining dynamic interactions, as reported in segmented copolymers with self-healing capabilities. The retention of mechanical integrity above the soft T_g is critical for self-healing, as it ensures that the material supports load-bearing while allowing polymer chain mobility sufficient to facilitate damage repair [26].

3.3.2. *Uniaxial tensile tests*

Fig. 6 shows the results of the tensile test conducted on the PU/TPU, comparing its mechanical properties to those of TPU. The PU/TPU results in a material with an impressive mechanical toughness of 106.45 MJ m^{-3}, tensile strengths reported up to 22.55 MPa, and an

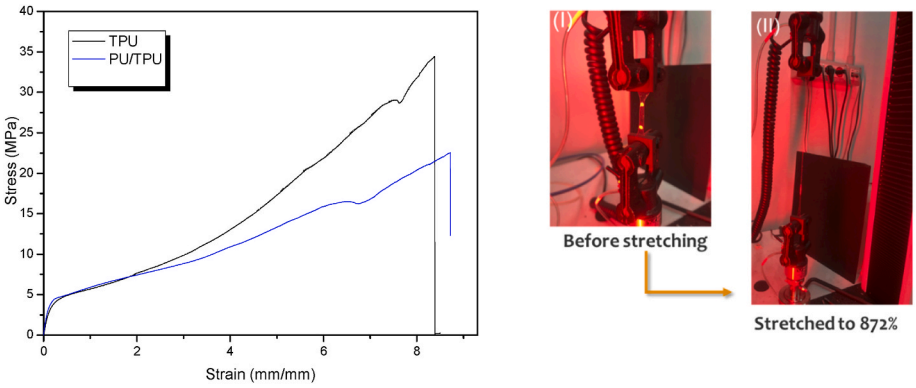

Fig. 6. Representative tensile stress-strain curves of neat TPU and PU/TPU.

elongation at break of 872%. In contrast, neat TPU, characterized by its segmented block copolymer structure, exhibits a tensile strength of 34.43 MPa and a substantial elongation at break of ~838%, owing to its rigid hard segments and flexible soft segments.

Those observed mechanical property variations between neat TPU and PU/TPU can be attributed to the complex interplay between phase morphology, interfacial interactions, and molecular mobility. Incorporating polyurea into the TPU matrix introduces a second phase, which can disrupt the crystalline structure of TPU, leading to a decrease in tensile strength to 22.55 MPa [27]. The presence of polyurea enhances the elongation at break (~872%) by increasing the mobility of polymer chains, facilitating larger deformation before rupture [28]. This improvement in ductility is attributed to the energy-dissipating properties of the polyurea phase and the increased amorphousness of the PU/TPU, which enables greater elastomeric deformation. These findings underscore the trade-off between strength and flexibility in polymer blends and highlight the importance of optimizing phase compatibility and morphology to achieve desired mechanical properties [26].

To investigate the effect of IPDI and TTE content on the mechanical properties of PU/TPU elastomers, samples were prepared with varying molar ratios of IPDI to TTE (1.5:1 and 0.5:1), Fig. 7.

The tensile stress and elongation at break of these samples revealed a clear dependence on the diisocyanate-to-chain extender ratio. For the 1.5:1 composition, the material exhibited a maximum tensile stress of 6.3 MPa and elongation at break of 789.5 %, whereas the 0.5:1 sample showed a higher tensile stress of 9.37 MPa and elongation of 858.2 %.

The tensile behavior of the PU/TPU elastomers reveals a clear trade-off between tensile strength and deformability as a function of polyurea content. Increasing the relative amount of polyurea leads to a moderate decrease in ultimate tensile strength, accompanied by a pronounced increase in elongation at break and overall toughness. This behavior indicates a transition from a strength-dominated response to a more ductile, energy-dissipative mechanical regime.

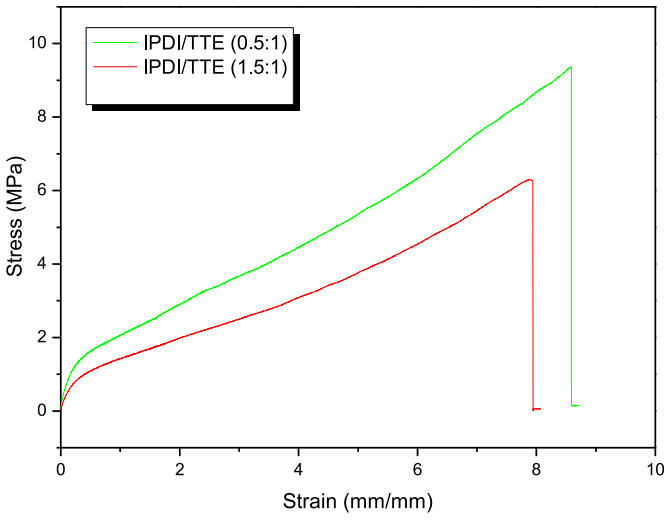

Fig. 7. Representative tensile stress-strain curves of IPDI/TTE (0.5:1). and IPDI/TTE (1.5:1).

Specifically, samples prepared with a higher IPDI/TTE ratio exhibit lower maximum tensile stress but enhanced strain at break, suggesting increased chain mobility and more effective stress redistribution during deformation. In contrast, formulations with lower polyurea content retain higher tensile strength, reflecting a greater contribution from load-bearing TPU domains. The optimized PU/TPU formulation used for self-healing tests combines these effects, achieving high tensile strength (up to 22.55 MPa) together with large elongation at break (≈872%), resulting in an exceptional mechanical toughness. From an application perspective, this balance between strength, extensibility, and toughness is particularly relevant for soft robotics and artificial skin systems, where materials are subjected to repeated large deformations rather than static load-bearing conditions. In such environments, increased ductility and damage tolerance are critical for long-term reliability. The presence of dynamic polyurea domains enables reversible hydrogen-bonding interactions that dissipate mechanical energy and promote self-healing, thereby compensating for the reduction in ultimate tensile strength and enhancing functional durability [8].

3.3.3. *Cyclic tensile tests*

The cyclic stress-strain responses of neat TPU and PU/TPU are shown in Fig. 8.

The PU/TPU elastomer exhibits a gradual decrease in peak stress from 4.02 MPa in the first cycle to 3.39 MPa after 50 cycles, corresponding to approximately 84% stress retention. In comparison, neat TPU shows a minor reduction in peak stress, from 4.10 MPa to 3.69 MPa, and retains about 90% of its initial stress. This difference suggests that incorporating polyurea segments introduces additional energy-dissipation pathways, leading to a more pronounced stress decay during repeated loading [29].

The higher stress retention observed in neat TPU can be attributed to its more homogeneous elastomeric network, which undergoes limited microstructural rearrangement under cyclic deformation [30]. In contrast, the PU/TPU displays larger hysteresis loops during the initial cycles, reflecting reversible bond dissociation, chain slippage, and redistribution of supramolecular interactions acting as sacrificial bonds [31]. Importantly, the hysteresis loop areas become nearly constant after the early cycles, suggesting that the dynamic network reaches a steady-state configuration in which both energy dissipation and mechanical response stabilize.

Overall, both materials withstand at least 50 consecutive damage-healing cycles without signs of catastrophic failure or mechanical collapse. While neat TPU exhibits higher stress retention and mechanical

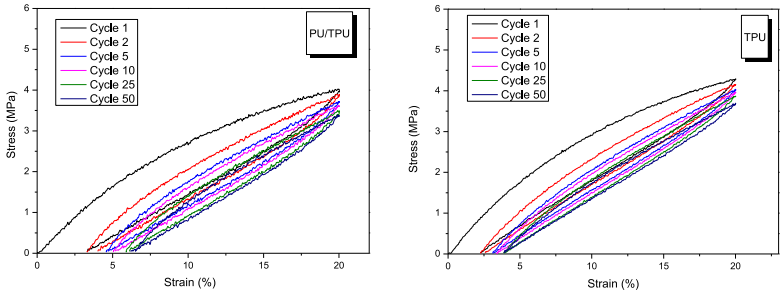

Fig. 8. Cyclic stress-strain responses of neat TPU and PU/TPU.

stability, the PU/TPU elastomer shows a stable mechanical response after initial accommodation, highlighting the self-healing mechanism's repeatability and long-term durability.

The cyclic stretch data were analyzed by plotting the maximum stress for each cycle, providing insight into the mechanical stability and long-term durability of PU/TPU under repeated tensile loading, as shown in Fig. 9.

The stress signal exhibits highly regular oscillations throughout the entire test duration, with well-defined stress peaks maintained across successive cycles. A slight reduction in peak stress is observed during the initial stage, attributed to molecular rearrangement and redistribution of dynamic supramolecular interactions within the PU/TPU network. Notably, after this initial accommodation phase, the stress response stabilizes, and no progressive decay or mechanical instability is detected over prolonged cycling.

The preservation of regular stress oscillations and the return of stress to near-zero between successive cycles confirm effective elastic recovery and the absence of significant permanent deformation accumulation.

3.4. Self-healing properties

3.4.1. Self-healing performance

The stress–strain behavior of the pristine and thermally healed PU/TPU elastomers is illustrated in Fig. 10.

The thermal treatment at 120 °C increased healing performance, with efficiencies of 34.4%, 76.8%, and 84.2% attained after 2, 5, and 10 min, respectively (Fig. 11a). This outcome underscores the rapid and

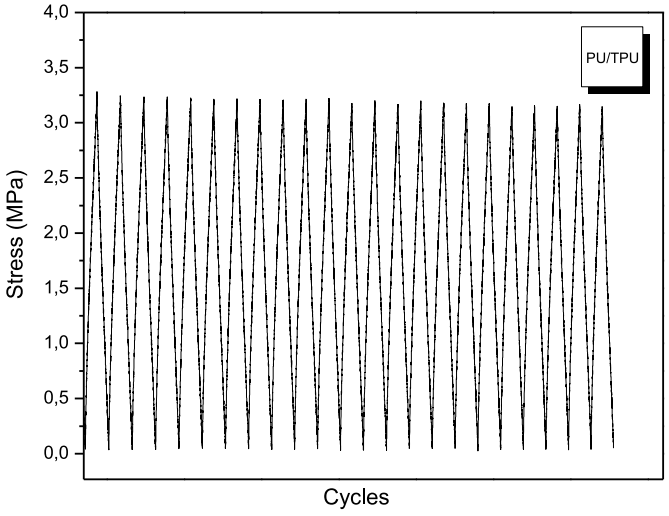

Fig. 9. Maximum stress of PU/TPU measured during cyclic stretch tests as a function of the number of loading cycles. Stress values are normalized to the first cycle to highlight the material's cyclic stability.

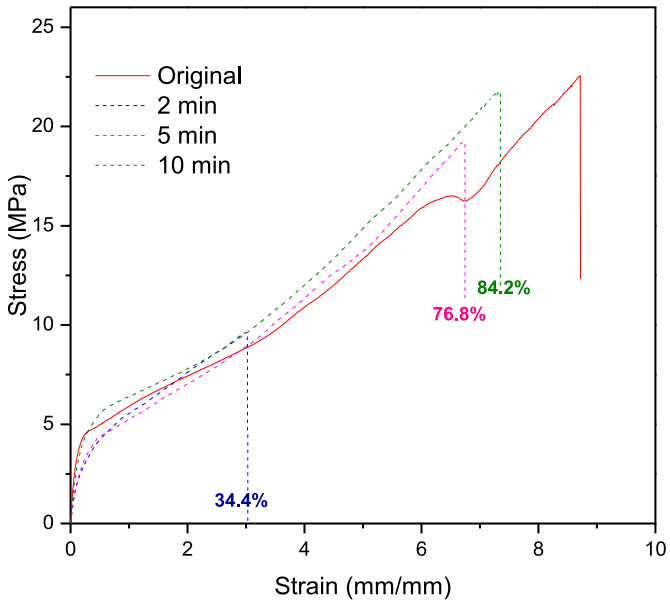

Fig. 10. Stress–strain curves of the polyurea/TPU film at three healing times.

effective self-repair capability of the PU/TPU system under thermal stimulus. In addition to its excellent self-healing performance, the PU/TPU elastomer also exhibits remarkable optical transparency, making it highly attractive for soft robotics applications that require visual monitoring or embedded sensing (Fig. 11b).

The neat TPU does not show measurable self-healing under the conditions investigated. The healing process is primarily governed by enhanced segmental mobility and the dynamic reformation of non-covalent interactions, particularly hydrogen bonding and urea exchange mechanisms, which are thermally activated [32,33] (Fig. 11c). The reversibility of hydrogen bonds plays a pivotal role in re-establishing interfacial cohesion across damaged regions.

The dynamic behavior of the PU/TPU system was investigated at different temperatures under 0.5 % of applied strain (Fig. 12a). The range of temperatures was chosen above the glass-to-rubbery transition between 35 °C and 55 °C. Stress-relaxation curves demonstrate that the PU/TPU system exhibits a faster decrease in stress with higher temperatures, because of enhanced mobility of PU chains and faster hydrogen bonding rearrangement. According to the Arrhenius equation, relaxation activation energy can be calculated by plotting the time corresponding to the value of 1/e of the initial stress against the reciprocal of temperature (Fig. 12b). The value of activation energy E_a obtained from the plot is 89.2 kJ/mol, which is comparable to other PU networks controlled by hydrogen bonds and exchangeable covalent bonds, such as urea or imines (55.2-109 kJ/mol) [34,35], but higher than other

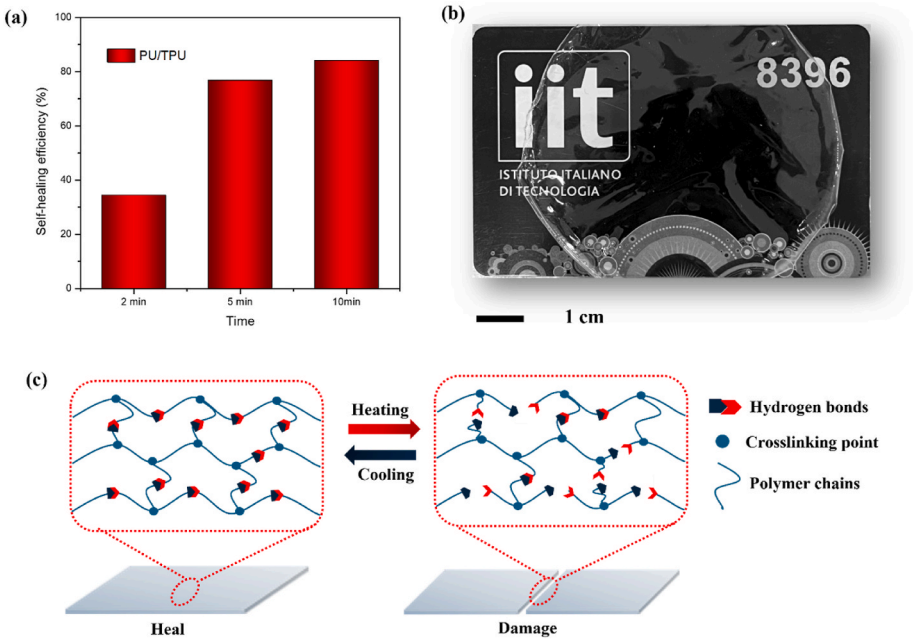

Fig. 11. (a) Self-healing efficiency of PU/TPU after self-healing for 2 min, 5 min, and 10 min at 120 °C. (b) Optical image of the dried transparent PU/TPU film. (c) Schematic of the thermally activated self-healing mechanism in the PU/TPU system, enabled by reversible dynamic interactions that allow network reconfiguration upon heating and structural recovery upon cooling.

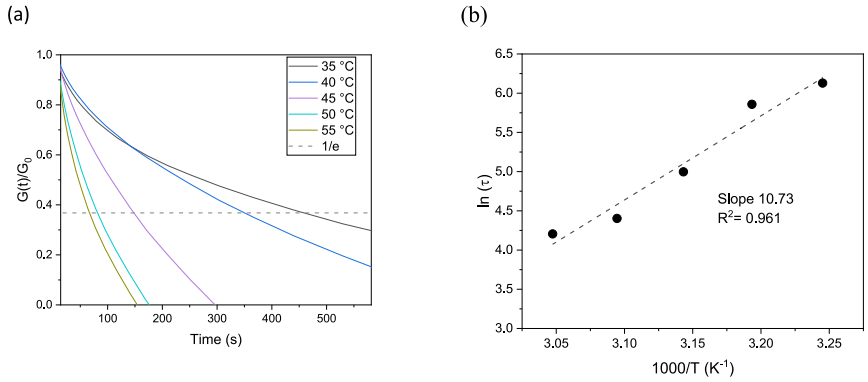

Fig. 12. (a) Stress-relaxation curves of PU/TPU system at different temperatures (range 35 °C-55 °C); (b) Arrhenius plot of relaxation times corresponding to a 1/e of the initial stress value.

polyurethane elastomers used in damping field (19-40 kJ/mol) [36]. The relatively high activation energy obtained for the PU/TPU system presented in this work may be due to reduced mobility of chain segments induced by ordered hydrogen bonding among the chains.

The mechanical properties before and after healing are shown in Table 1, which evidences a progressive recovery in tensile performance as a function of healing duration. These results confirm the capacity of the PU/TPU network to balance mechanical robustness with intrinsic self-healing functionality. Moreover, the isophorone diisocyanate (IPDI)-based hard segments were instrumental in dissipating mechanical stress and enabling reversible supramolecular interactions, which are critical for efficient damage repair [14].

Compared with previously reported self-healing systems [30,31,37–41] (Fig. 13), the high toughness and rapid self-healing highlight the potential of PU/TPU as a promising material for high-performance self-healing elastomers.

Table 1
Mechanical properties of PU/TPU before damage (pristine) and after healing at 120 °C for different time intervals.

Healed time	Toughness (MJ m^{-3})	Elongation at break (%)	Tensile strength (MPa)
Original	106.45	872	22.55
2 min	-	300	9.66
5 min	69.41	670	19.23
15 min	87.87	879	21.76

3.4.2. *Optical microscopy images*

PU/TPU self-healing was also investigated using an optical microscope. Fig. 14 shows the healing of the surface scratches of PU/TPU at 120 °C. The scratch gradually disappeared with time.

Additionally, an analysis of the images was conducted to investigate the behavior of the crack section and the full width at half maximum (FWHM) during the healing process. The resulting plot (Fig. 15) presents

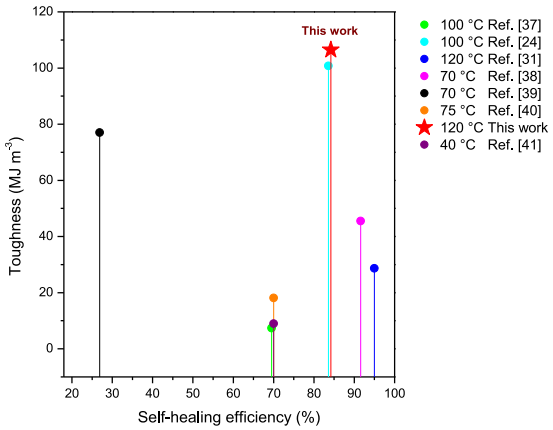

Fig. 13. Comparison of the self-healing efficiency and toughness of PU/TPU reported in this work with those reported in other literature references, with healing temperatures of the literature data ranging from 40 to 120 °C.

healing time on the x-axis, with multiple y-axes depicting peak section area, height, and FWHM. Temperature was extracted from real-time thermography, and peak features from the optical profile are shown in Fig. 16.

These data provide a real-time morphological signature of the healing dynamics. The progressive increase in section area over time suggests enhanced chain interdiffusion and supramolecular reorganization, while the concurrent decrease in FWHM indicates a more defined and cohesive interfacial region as the damage is progressively repaired. These morphological trends correlate with mechanical recovery data from tensile testing discussed previously in this study, further supporting the role of thermal energy in facilitating reversible hydrogen bonding and structural reorganization within the PU/TPU matrix.

The evolution of peak morphology as a function of heating time provides critical insights into the efficiency and mechanism of self-healing in the PU/TPU system. The increase in peak height and area up to ~117.9 °C in a time of 92 s reflects a thermally induced enhancement in segmental mobility and chain interdiffusion at the damaged interface. This is consistent with the expected behavior of hydrogen-bonded networks, in which thermal activation facilitates the reversible dissociation and reformation of supramolecular interactions, such as urea–urea hydrogen bonds, which are known to govern self-healing behavior [42,43]. In this context, the gradual increase in peak height indicates effective chain reorganization and re-entanglement, critical steps toward mechanical reconnection across the damaged area. This dynamic reconfiguration enables the restoration of mechanical properties, as previously observed in tensile tests, where healing efficiency increases significantly with time under similar thermal conditions [44]. However, beyond the critical temperature around 121.5 °C, the sudden decrease in both peak height and area, coupled with the increase in FWHM, suggests a breakdown in structural integrity. This may result from excessive chain mobility or partial melting, which disrupts the physical crosslinks and prevents effective reconnection of polymer chains, thus limiting healing performance. Therefore, the data confirms that self-healing efficiency is strongly temperature-dependent, governed by an optimal window in which polymer chains gain sufficient mobility to rearrange and re-establish interfacial interactions, without losing the cohesive structure necessary for healing [45,46]. This highlights the importance of optimizing the healing conditions, particularly the temperature and activation time, to achieve maximum recovery in supramolecular polymer systems.

4. Conclusions

In this study, we developed a PU/TPU elastomer that combines high mechanical performance with fast, efficient self-healing, enabled by a synergistic architecture of soft TPU domains and hard polyurea/urethane segments. Spectroscopic and dynamic mechanical analyses confirmed a dynamic hydrogen-bond network and a dual-T_g, microphase-separated structure that balances chain mobility for healing with mechanical reinforcement at higher temperatures. The material exhibits a tensile strength of 22.55 MPa, elongation at break of 872 %, toughness of 106.45 MJ m^{-3}, and stable cyclic response over 50 loading cycles, indicating robust, repeatable performance. Under thermal activation at 120 °C, healing efficiencies of 34.4 %, 76.8 %, and 84.2 % were achieved after 2, 5, and 10 min, respectively, with an activation energy of 89.2 kJ mol^{-1} pointing to a thermally activated rearrangement of hydrogen-bonded networks. Overall, the commercial TPU provides a load-bearing, elastic matrix, while the supramolecular polyurea/urethane network supplies reversible bonding and energy dissipation,

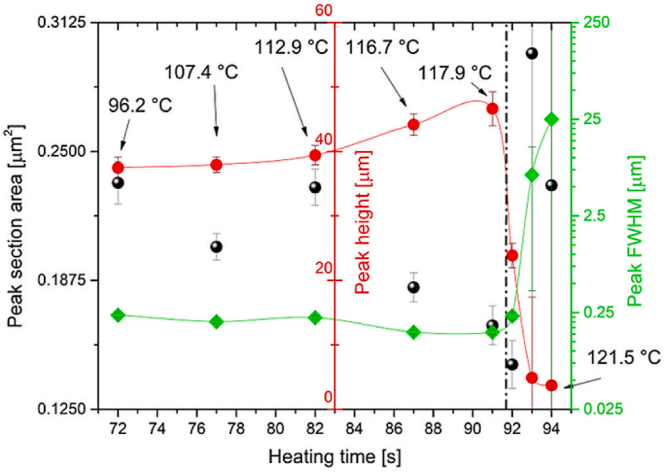

Fig. 15. Variation of peak section area and FWHM with healing time. The x-axis represents healing time, the y-axis (left, black dots) shows peak section area, (middle, red dots and curve) the peak height, and (right, green dots and curve) the FWHM, reflecting the morphological evolution during the self-healing process in the PU/TPU system.

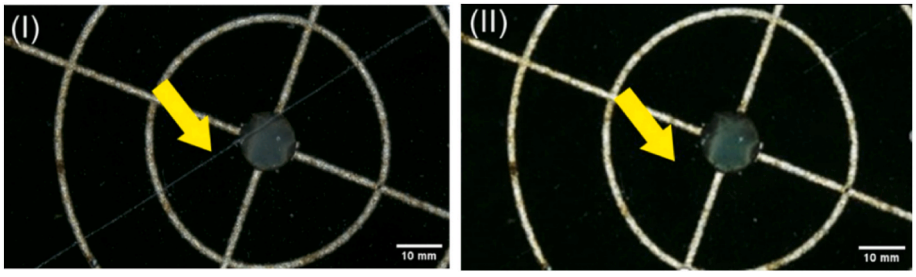

Fig. 14. Images of PU/TPU damaged and healed.

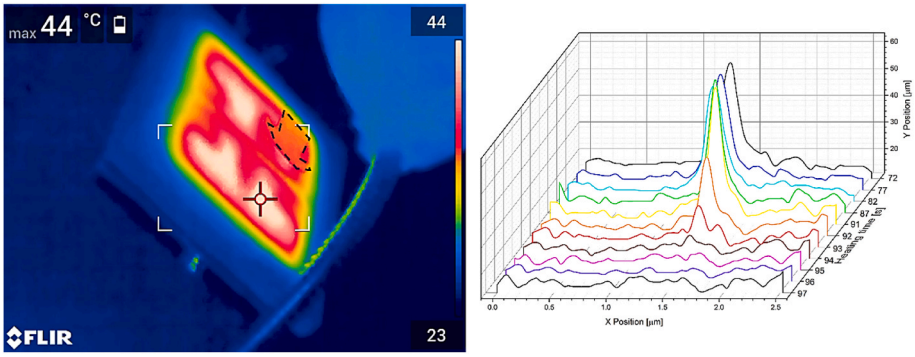

Fig. 16. Thermography of the sample showing the heated stage under the microscope and the position of the damaged specimen, indicated by the black dashed line (left). Optical profiles of the crack healing process, taking place between 72 s and 95 s of heating time at 120 °C.

yielding a material that withstands large strains and autonomously repairs damage—suited for soft robotics, artificial skin, and wearable devices. Future work should target self-healing at lower temperatures, further optimization of hard-segment architecture, integration of functional fillers (e.g. for sensing or actuation), and long-term testing under realistic operating conditions.

CRediT authorship contribution statement

Adriana Nunes dos Santos: Conceptualization, Data curation, Investigation, Methodology, Validation, Visualization, Writing – original draft, Writing – review & editing. **Mattia Pesce:** Investigation, Writing – review & editing. **Luca Ceseracciu:** Investigation, Writing – original draft, Writing – review & editing. **Martina Nardi:** Data curation, Investigation, Writing – review & editing. **Francesca Vasile:** Data curation, Investigation, Writing – review & editing. **Ermelinda Falletta:** Data curation, Investigation, Writing – review & editing. **Alessandro Chiolerio:** Conceptualization, Funding acquisition, Investigation, Methodology, Project administration, Resources, Supervision, Validation, Writing – original draft, Writing – review & editing.

Declaration of competing interest

The authors declare that they have no known competing financial interests or personal relationships that could have appeared to influence the work reported in this paper.

Acknowledgments

This work has received funding from the European Innovation Council and SMEs Executive Agency (EISMEA) under grant agreement no. 964388. Nuclear Magnetic Resonance analyses were performed at the NMR facility of the Unitech COSPECT at the University of Milan (Italy).

Data availability

Data will be made available on request.

References

[1] R.S. Srivastav, A.P. More, A comprehensive review of self-healing polymers: mechanisms, types, and industry implications, Polym. Adv. Technol. 36 (2025) 1–17, https://doi.org/10.1002/pat.70092.
[2] S. Kim, H. Jeon, J.M. Koo, D.X. Oh, J. Park, Practical applications of self-healing polymers beyond mechanical and electrical recovery, Adv. Sci. 11 (2024) 1–22, https://doi.org/10.1002/advs.202302463.
[3] S. Utrera-Barrios, R. Verdejo, M.Á. López-Manchado, M. Hernández Santana, Self-healing elastomers: a sustainable solution for automotive applications, Eur. Polym. J. 190 (2023) 112023, https://doi.org/10.1016/j.eurpolymj.2023.112023.
[4] A. Nunes, R.J. De Oliveira, A. Chiolerio, Plasmonic nanostructures for enhanced self-healing in materials : a review, ACS Omega (2025), https://doi.org/10.1021/acsomega.5c03274.
[5] Y. Hao, G. Zhu, B. Li, Self-healing polyurethane-urea elastomers with high strength and toughness based on dynamic hindered urea bonds and hydrogen bonds, Ind. Eng. Chem. Res. 63 (2024) 19350–19358, https://doi.org/10.1021/acs.iecr.4c02340.
[6] P. Wu, H. Cheng, X. Wang, R. Shi, C. Zhang, M. Arai, F. Zhao, A self-healing and recyclable polyurethane-urea diels-Alder adduct synthesized from carbon dioxide and furfuryl amine, Green Chem. 23 (2021) 552–560, https://doi.org/10.1039/d0gc03695a.
[7] Z. Zhou, X. Wang, H. Yu, C. Yu, F. Zhang, Dynamic cross-linked polyurea/polydopamine nanocomposites for photoresponsive self-healing and photoactuation, Macromolecules 55 (2022) 2193–2201, https://doi.org/10.1021/acs.macromol.1c02534.
[8] L. Zhang, D. Wang, L. Xu, X. Zhang, A. Zhang, Y. Xu, A highly stretchable, transparent, notch-insensitive self-healing elastomer for coating, J. Mater. Chem. C 8 (2020) 2043–2053, https://doi.org/10.1039/c9tc05612b.
[9] D. Khanh, S. Veeralingam, J. Kim, Self-repairing thermoplastic polyurethane-based triboelectric nanogenerator with molybdenum disulfide charge-trapping for advanced wearable devices, Nano Energy 127 (2024) 109714, https://doi.org/10.1016/j.nanoen.2024.109714.
[10] Y. Hao, G. Zhu, The latest advances in mechanically robust self-healing polyurea based on dynamic chemistry, Adv. Sci. (2025) 2414788, https://doi.org/10.1002/advs.202414788.
[11] Y. Li, M. Zhou, R. Wang, H. Han, Z. Huang, J. Wang, Self-healing polyurethane elastomers: an essential review and prospects for future research, Eur. Polym. J. 214 (2024) 113159, https://doi.org/10.1016/j.eurpolymj.2024.113159.
[12] Y. Zhang, C. Xiong, X. Ma, X. Zhang, J. Yin, S. Xu, Z. Fan, Y. Qin, Y. Liu, Low-temperature self-healing supramolecular Zinc-Poly(Urea-Urethane) elastomer, ACS Appl. Polym. Mater. 6 (2024) 4525–4534, https://doi.org/10.1021/acsapm.3c03211.
[13] T. Chen, L. Fang, X. Li, D. Gao, C. Lu, Z. Xu, Self-healing polymer coatings of polyurea-urethane/epoxy blends with reversible and dynamic bonds, Prog. Org. Coating 147 (2020) 105876, https://doi.org/10.1016/j.porgcoat.2020.105876.
[14] T. Li, T. Zheng, J. Han, Z. Liu, Z.X. Guo, Z. Zhuang, J. Xu, B.H. Guo, Effects of diisocyanate structure and disulfide chain extender on hard segmental packing and self-healing property of polyurea elastomers, Polymers (Basel) 11 (2019) 838, https://doi.org/10.3390/polym11050838.
[15] A.K. Padhan, D. Mandal, Types of Chemistries Involved in self-healing Polymeric Systems, INC, 2020, https://doi.org/10.1016/B978-0-12-818450-9.00002-7.
[16] Y. Ren, X. Dong, Dynamic polymeric materials via hydrogen-bond cross-linking: effect of multiple network topologies, Prog. Polym. Sci. 158 (2024) 101890, https://doi.org/10.1016/j.progpolymsci.2024.101890.
[17] B.C.K. Tee, C. Wang, R. Allen, Z. Bao, An electrically and mechanically self-healing composite with pressure- and flexion-sensitive properties for electronic skin applications, Nat. Nanotechnol. 7 (2012) 825–832, https://doi.org/10.1038/nnano.2012.192.
[18] E. Roels, S. Terryn, F. Iida, A.W. Bosman, S. Norvez, F. Clemens, G. Van Assche, B. Vanderborght, J. Brancart, Processing of self-healing polymers for soft robotics, Adv. Mater. 34 (2022) 1–27, https://doi.org/10.1002/adma.202104798.
[19] A. Chiolerio, M.B. Quadrelli, Smart fluid systems: the advent of autonomous liquid robotics, Adv. Sci. 4 (2017) 1700036, https://doi.org/10.1002/advs.201700036.
[20] X. Shen, Z. Dong, C. Sim, Y. Li, A comparative study on the self-healing characterizations and formulation optimization of polyurea coating, Polymers (Basel) 14 (2022) 1–16, https://doi.org/10.3390/polym14173520.
[21] J. Wang, S. Hu, B. Yang, G. Jin, X. Zhou, X. Lin, R. Wang, Y. Lu, L. Zhang, Novel three-dimensional-printing strategy based on dynamic urea bonds for isotropy and mechanical robustness of large-scale printed products, ACS Appl. Mater. Interfaces 14 (2022) 1994–2005, https://doi.org/10.1021/acsami.1c20659.
[22] Z. Zhang, M. Zhang, G. Yan, M. Li, H. Ji, Y. Feng, X. Qu, X. Hu, X. Zhang, Accelerated oxidation-reduction kinetic functional polyurea binders: diselenide building block as redox co-moderators, Chem. Eng. J. 489 (2024) 151288, https://doi.org/10.1016/j.cej.2024.151288.

[23] J. Hu, R. Mo, X. Jiang, X. Sheng, X. Zhang, Towards mechanical robust yet self-healing polyurethane elastomers via combination of dynamic main chain and dangling quadruple hydrogen bonds, Polymer (Guildf). 183 (2019) 121912, https://doi.org/10.1016/j.polymer.2019.121912.
[24] N. Li, Y. Wang, J. You, Z. Jiang, Y. Wang, H. Xing, M. Li, Influence of reaction-induced microphase-separation structure on mechanical properties , shape memory , and recyclable performance of EVA − polyurea nanocomposite, Macromolecules 58 (2025) 12466–12475, https://doi.org/10.1021/acs.macromol.5c01922.
[25] V. Shahi, V. Alizadeh, A.V. Amirkhizi, Thermo-mechanical characterization of polyurea variants, Mech. Time-Dependent Mater. 25 (2021) 447–471, https://doi.org/10.1007/s11043-020-09454-0.
[26] Y. Hao, G. Zhu, B. Li, Mechanically robust and self-healable polyureas based on multiple dynamic bonds, Ind. Eng. Chem. Res. 62 (2023) 10444–10453, https://doi.org/10.1021/acs.iecr.3c00693.
[27] Y. He, D. Xie, X. Zhang, The structure, microphase-separated morphology, and property of polyurethanes and polyureas, J. Mater. Sci. 49 (2014) 7339–7352, https://doi.org/10.1007/s10853-014-8458-y.
[28] S. Wang, Y. Yang, H. Ying, X. Jing, B. Wang, Y. Zhang, J. Cheng, Recyclable, self-healable, and highly malleable poly(urethane-urea)s with improved thermal and mechanical performances, ACS Appl. Mater. Interfaces 12 (2020) 35403–35414, https://doi.org/10.1021/acsami.0c07553.
[29] C. Kang, L. Gao, H. Zhu, C. Lang, J. Jiang, J. Wei, Adsorption of Hg(II) in solution by mercaptofunctionalized palygorskite, Environ. Sci. Pollut. Res. 28 (2021) 66287–66302, https://doi.org/10.1007/S11356-021-15637-0/TABLES/5.
[30] Y. Song, J. Li, G. Song, X. Li, Tough and self-healing waterborne polyurethane elastomers via dynamic hydrogen bonds design for flexible conductive substrate applications, ACS Appl. Mater. Interfaces 16 (2024) 2683–2691, https://doi.org/10.1021/acsami.3c12688.
[31] P. Wu, H. Cheng, Y. Wang, R. Shi, Z. Wu, M. Arai, F. Zhao, New kind of thermoplastic polyurea elastomers synthesized from CO2and with self-healing properties, ACS Sustain. Chem. Eng. 8 (2020) 12677–12685, https://doi.org/10.1021/acssuschemeng.0c04732.
[32] P. Du, X. Liu, Z. Zheng, X. Wang, T. Joncheray, Y. Zhang, Synthesis and characterization of linear self-healing polyurethane based on thermally reversible diels-alder reaction, RSC Adv. 3 (2013) 15475–15482, https://doi.org/10.1039/c3ra42278j.
[33] X. Chen, S. Zhao, A. Yuan, S. Chen, Y. Liao, X. Fu, J. Lei, L. Jiang, Enabling the epoxy-based polyurea with adjustable mechanical properties, recyclability, and 3D shape configuration, Macromolecules 57 (2024) 294–304, https://doi.org/10.1021/acs.macromol.3c01688.
[34] F. Elizalde, J. Amici, S. Trano, G. Vozzolo, R. Aguirresarobe, D. Versaci, S. Bodoardo, D. Mecerreyes, F. Bella, Self-healable dynamic poly(urea-urethane) gel electrolyte for lithium batteries, J. Mater. Chem. 10 (2022) 12588–12596, https://doi.org/10.1039/d2ta02239g.
[35] X. Du, L. Shuai, S. Wang, H. Wu, J. Li, J. Wen, M. Zhu, J. Hu, Y. Nie, Polymer chemistry special interplay of hydrogen bonds and dynamic vitrimers with excellent recyclability and, Polym. Chem. 16 (2025) 4040–4053, https://doi.org/10.1039/d5py00728c.
[36] X. Han, D. Wang, X. Chen, S. Nie, C. Huyan, D. Liu, F. Chen, High damping polyurethane elastomers with wide temperature ranges, Polymer (Guildf). 325 (2025) 128307, https://doi.org/10.1016/j.polymer.2025.128307.
[37] P.F. Cao, B. Li, T. Hong, J. Townsend, Z. Qiang, K. Xing, K.D. Vogiatzis, Y. Wang, J. W. Mays, A.P. Sokolov, T. Saito, Superstretchable, self-healing polymeric elastomers with tunable properties, Adv. Funct. Mater. 28 (2018) 1–9, https://doi.org/10.1002/adfm.201800741.
[38] L. Lu, J. Xu, J. Li, Y. Xing, Z. Zhou, F. Zhang, High-toughness and intrinsically self-healing cross-linked polyurea elastomers with dynamic sextuple H-Bonds, Macromolecules 57 (2024) 2100–2109, https://doi.org/10.1021/acs.macromol.3c02202.
[39] Y. Eom, S.M. Kim, M. Lee, H. Jeon, J. Park, E.S. Lee, S.Y. Hwang, J. Park, D.X. Oh, Mechano-responsive hydrogen-bonding array of thermoplastic polyurethane elastomer captures both strength and self-healing, Nat. Commun. 12 (2021) 1–11, https://doi.org/10.1038/s41467-021-20931-z.
[40] X. Xun, Z. Zhang, X. Zhao, B. Zhao, F. Gao, Z. Kang, Q. Liao, Y. Zhang, Highly robust and self-powered electronic skin based on tough conductive self-healing elastomer, ACS Nano 14 (2020) 9066–9072, https://doi.org/10.1021/acsnano.0c04158.
[41] B. Li, S. Ge, X. Zhao, Q. Chen, J. Tian, D. Hun, A.P. Sokolov, T. Saito, P.F. Cao, Well-tunable, 3D-printable, and fast autonomous self-healing elastomers, Supramol. Mater. 2 (2023) 100042, https://doi.org/10.1016/j.supmat.2023.100042.
[42] J. Xu, X. Wang, X. Zhang, Y. Zhang, Z. Yang, S. Li, L. Tao, Q. Wang, T. Wang, Room-temperature self-healing supramolecular polyurethanes based on the synergistic strengthening of biomimetic hierarchical hydrogen-bonding interactions and coordination bonds, Chem. Eng. J. 451 (2023) 138673, https://doi.org/10.1016/j.cej.2022.138673.
[43] J. Liu, J. Liu, S. Wang, J. Huang, S. Wu, Z. Tang, B. Guo, L. Zhang, An advanced elastomer with an unprecedented combination of excellent mechanical properties and high self-healing capability, J. Mater. Chem. A 5 (2017) 25660–25671, https://doi.org/10.1039/c7ta08255j.
[44] Z. Li, Z. Cao, Q. Zhao, S. Mei, Y. Zhang, W. Zhao, X. Li, X. Zhang, Z. Cui, P. Fu, X. Pang, M. Liu, Self-healing and shape memory reconfigurable poly(urethane-urea-amide) elastomers containing multiple dynamic bonds for improving performance of 4D printout, Chem. Eng. J. 485 (2024) 149933, https://doi.org/10.1016/j.cej.2024.149933.
[45] A. Jiménez-Suárez, G. Buendía Sánchez, S.G. Prolongo, Temperature-dependent synergistic self-healing in thermoplastic-thermoset blends: unraveling the role of thermoplastics and dynamic covalent networks, J. Mater. Res. Technol. 29 (2024) 550–557, https://doi.org/10.1016/j.jmrt.2024.01.089.
[46] J. Chen, F. Li, Y. Luo, Y. Shi, X. Ma, M. Zhang, D.W. Boukhvalov, Z. Luo, A self-healing elastomer based on an intrinsic non-covalent cross-linking mechanism, J. Mater. Chem. A 7 (2019) 15207–15214, https://doi.org/10.1039/c9ta03775f.